Hydrothermal synthesis of Yb^{3+}, Tm^{3+} co-doped Gd_6MoO_{12} and its upconversion properties*

Di Qiu-Mei(邸秋梅), Sun Yu-Mei(孙宇梅), Xu Qi-Guang(徐齐光), Han Liu(韩 柳), Xue Bing(薛 兵), and Sun Jia-Yue(孙家跃)†

School of Science, Beijing Technology and Business University, Beijing 100048, *China*

(Received 15 December 2014; revised manuscript received 22 January 2015; published online 10 April 2015)

Yb^{3+}, Tm^{3+} co-doped Gd_6MoO_{12} phosphors with different morphologies are prepared by the hydrothermal method. The dendrites present different morphologies (including hexagonal prisms, spindles, and spheres) after changing the pH value and edetate disodium (EDTA) usage. It is found that each of the two factors plays a crucial role in forming different morphologies.

The up-conversion (UC) luminescence is studied. Under 980-nm semiconductor laser excitation, relatively strong blue emission and weak red emission are observed. Finally, the effect of pumping power on the UC luminescence properties and the level diagram mechanism of Gd_6MoO_{12}:Yb^{3+}/Tm^{3+} phosphor are also discussed.

Keywords: hydrothermal synthesis, morphologies, upconversion luminescence

PACS: 78.20.–e, 65.80.–g, 81.05.–t **DOI:** 10.1088/1674-1056/24/6/067801

1. Introduction

In recent years, much attention has been paid to the infrared-to-visible up-converted luminescence (UCL) in rare-earth (RE) ions-doped phosphors due to their potential applications in biological fluorescent labels, color displays and infrared sensors.[1–7] These applications are highly dependent on size, morphology, structure, and other fundamental factors which govern the luminescence behaviors.[8] Therefore, the synthesis of materials doped with rare earths has received more and more attention. So far, many reports have been published on the study of RE-doped tungstate and molybdate matrix, due to their highly chemically, photo-thermally, photochemically stable properties.[9,10] These materials were synthesized through various methods, such as the high temperature solid method, the sol–gel method, and the hydrothermal method. The hydrothermal method has the advantages in preparing various inorganic materials, such as less pollution, higher homogeneity and purity, and more controllable morphologies.[11–13] The variations of conditions in the synthesis process, such as pH, annealing temperature, and the addition of different chelators (citric acid or EDTA) may result in the formation of different morphologies of the final samples, and may further influence the phosphor luminescence properties.

Here in this paper, Yb^{3+}, Tm^{3+} co-doped Gd_6MoO_{12} powders are synthesized via a hydrothermal method. The samples are characterized by x-ray diffraction (XRD), scanning electron microscopy (SEM), thermogravimetry — differential thermal analysis (TG-DSC), and upconversion (UC) emission spectra.

2. Experiment

2.1. Starting materials

The $Gd_{5.74}MoO_{12}$:$0.25Yb^{3+}$, $0.01Tm^{3+}$ samples were prepared by the hydrothermal method. The starting materials were $(NH_4)_6Mo_7O_{24}\cdot 4H_2O$ (99.0%), Tm_2O_3 (99.99%), Gd_2O_3 (99.99%), Yb_2O_3 (99.99%), HNO_3(65%–68%), and $C_{10}H_4N_2O_8Na_2\cdot 2H_2O$ (EDTA) (A.R.). All chemicals were directly used without further purification.

2.2. Preparation of Tm^{3+}/Yb^{3+} co-doped Gd_6MoO_{12}

The Tm^{3+}/Yb^{3+} co-doped Gd_6MoO_{12} was synthesized by a facial solution phase precipitation reaction. In a typical synthesis, solutions of Tm $(NO_3)_3$, Yb $(NO_3)_3$, and Gd $(NO_3)_3$ were prepared by dissolving stoichiometric Tm_2O_3, Gd_2O_3, and Yb_2O_3 separately in dilute HNO_3 as stock solutions, respectively. EDTA and Mo^{6+} were obtained by dissolving stoichiometric $C_{10}H_4N_2O_8Na_2\cdot 2H_2O$ and $(NH_4)_6Mo_7O_{24}\cdot 4H_2O$ powder separately in the deionized water ($n_{EDTA}/n_{Ln}^{3+} = 1$). In the next moment, appropriate amounts of $Re(NO_3)_3$ (Re^{3+} = Yb^{3+}, Tm^{3+}, Gd^{3+}) and Mo^{6+} were mixed under vigorous stirring for 30 min. Samples A and B were obtained by adjusting the pH values of 3 and 9 respectively with diluted $NH_3\cdot H_2O$. Sample C was obtained by adding the EDTA into the parallel sample A. Finally, the as-obtained mixing solutions were transferred into a 50-

*Project supported by the National Natural Science Foundation of China (Grant No. 20976002), the Beijing Natural Science Foundation, China (Grant No. 2122012), the Key Projects for Science and Technology of Beijing Education Commission, China (Grant No. KZ201310011013), and the Education and Research Fund of Guangdong Province, China (Grant No. 2011B090400100).

†Corresponding author. E-mail: jiayue_sun@126.com

© 2015 Chinese Physical Society and IOP Publishing Ltd

ml teflon bottle held in a stainless steel autoclave, sealed and maintained at the selected temperature of 200 °C for 20 h. As the autoclave cooled to room temperature naturally, the precipitates were separated by centrifugation, washed with ethanol and deionized water in sequence three times, and dried in a vacuum at 80 °C for 12 h. Sample D was obtained by further calcinating precursor (a) at 700 °C for 4 h.

2.3. Characterization

The structures of the phosphors were analyzed on a Shimadzu model XRD-6000 x-ray powder diffraction with Cu $K\alpha$ radiation, 40 kV, 30 m A. The XRD patterns were recorded in the range of $18^\circ < 2\theta < 80^\circ$. Its room temperature upconversion emission spectra were recorded by using a FluoroLog-3 spectrophotometer (HORIBAJOBINYVON USA) equipped with an external power-controllable 980-nm semiconductor laser. The morphologies of the samples were recorded using a scanning electron microscope (SEM, JEOL and JSM-6490). Thermogravimetry — differential thermal analysis (TG-DSC) was performed on a Setaram TGA 92 TG-DSC instrument at a heat rate of 10 °C/min from room temperature to a maximum temperature of 950 °C.

3. Results and discussion

3.1. Phase identification and morphologies

The typical XRD patterns of the prepared products A, B, C are shown in Fig. 1(a). The diffraction peaks of samples obtained under different conditions can be exactly assigned to the pure Gd_6MoO_{12} crystal [JCPDS Card: No. 24-1085], indicating that the crystal lattice and basic structure of the Gd_6MoO_{12} host can be obtained by the above method.

Figure 1 shows the SEM images of the $Gd_{5.74}MoO_{12}$:$0.25Yb^{3+}$, $0.01Tm^{3+}$ samples under different synthesis conditions. Figure 1(b), obtained at a pH value of 3, presents the morphology of long hexagonal prism with an average length of about 50 μm. When the pH value is 9, the spindle-like shape is obtained as shown in Fig. 1(c). The above information indicates that the pH values are responsible for the uniform morphologies.

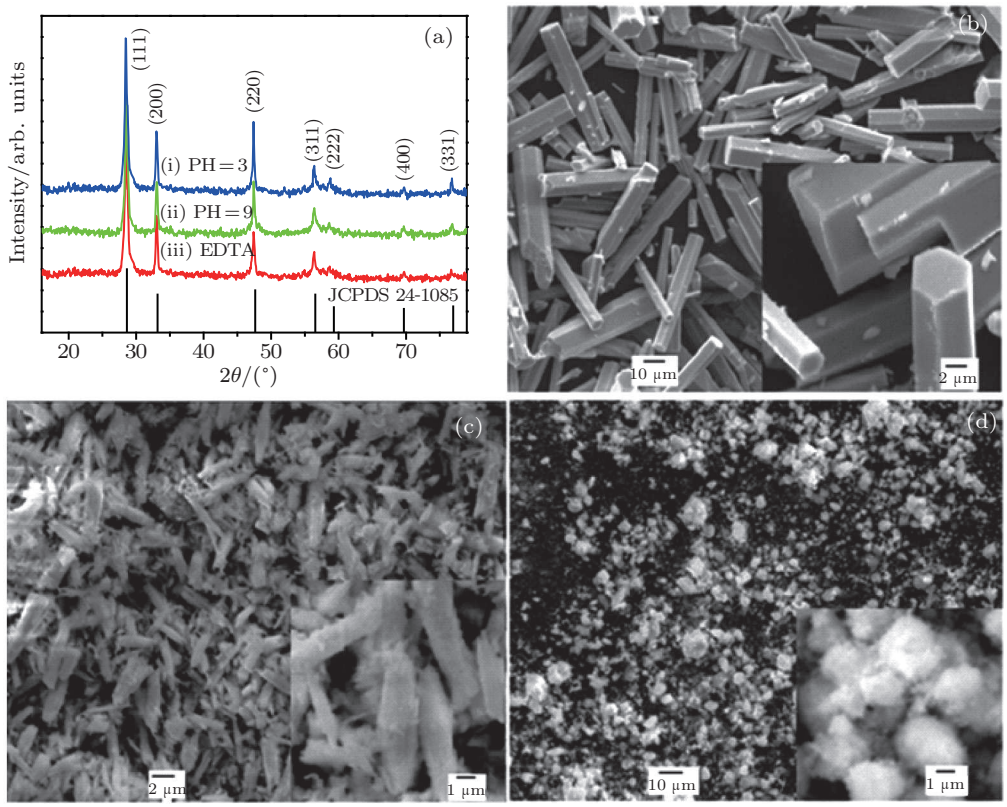


Fig. 1. (color online) (a) The x-ray diffraction patterns of Gd_6MoO_{12}:Yb^{3+}/Tm^{3+} samples obtained under different conditions: (i) pH = 3, (ii) pH = 9, (iii) pH = 3/EDTA; SEM images of Gd_6MoO_{12}:Yb^{3+}/Tm^{3+} samples obtained at different conditions: (b) pH = 3, (c) pH = 9, and (d) pH = 3/EDTA.

The crystal growth process has already been studied a lot in the past decades.[14–16] The high ratio of height to side length indicates that the growth rate of the prismatic facets is quicker than that of top and bottom facets in an acidic condition. As in an alkalinity condition, the spindle shape appears and the average size becomes smaller. This may be due to the fact that the growths of the length and the side facets have been prevented in the alkalinity condition. The shape chang-

ing can be explained as controlling the relative growth rates in different directions by varying pH values.

Here, EDTA is selected as the chelator due to its efficiency in controlling the crystal morphologies.[17,18] The structure stability coefficient of EDTA with Ln^{3+} ions is larger than that of citric acid, ascribing to its six binding sites and ring-like space structure.[19] As shown in Fig. 1(d), sphere-like morphology with an average length of about 5 μm can be seen, which is obtained by mixing EDTA into the solution with a pH value of 3. The sphere-like particle appearance indicates that the sequestering effects of EDTA on all directions are completely uniform. The synthesized crystals above are all comprised of the same lanthanide dopants.

In a word, the differences in growth rate among various crystal facets result in the different morphologies of the crystallite. The relatively fast rate of crystal growth has the smaller area of crystal facet perpendicular to this growth direction.[5]

To further study the annealing influences on the morphology and structure, sample D is obtained by annealing sample A at 700 °C for 4 h. The XRD pattern of sample D is shown in Fig. 2(a). The phase peaks are consistent with the standard data of Gd_6MoO_{12}, indicating that the Gd_6MoO_{12} crystal is obtained successfully. The SEM image of sample D is shown in Fig. 2(b). The relatively small size of grain in sample D compared with the size of grain in sample A indicates that the heating process breaks the crystal to some extent. In addition, by comparing the XRD patterns with those of sample A in Fig. 1, we can observe that sample D has stronger peaks and narrow phase width, which implies much higher crystallinity than in sample A.

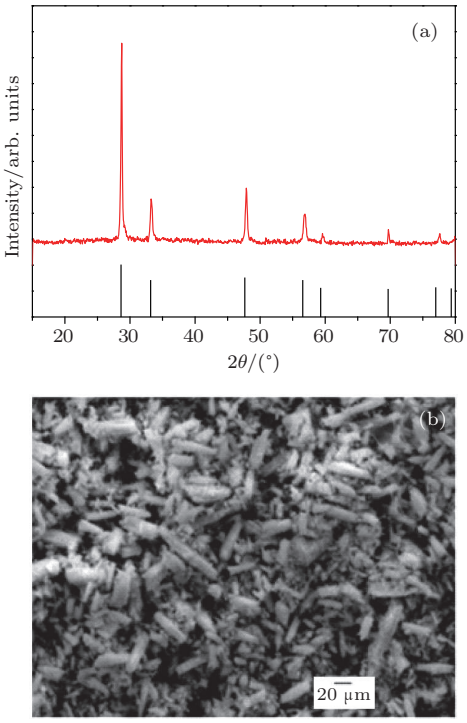


Fig. 2. (color online) (a) XRD patterns of sample D; (b) the SEM image of sample D.

3.2. TG-DSC analysis of the precursors

The TG-DSC analysis is made to understand the crystallization process of the precursor A from room temperature to a maximum temperature of 950 °C.

As shown in Fig. 3, the weight loss of sample A occurs with increasing temperature up to about 665 °C. Based on the DSC curve, the decomposition and crystallization processes of the precursor can be divided into three stages. The first stage is from 50 °C to 275 °C, in which the sample loses 2% gross weight. This stage is corresponding to the volatilization of the absorbed water and the decomposition of the precursors.[11] The second stage shows a large loss of 15% when temperature increases from 275 °C to 665 °C. In this stage, the mass loss should correspond to the decomposition of metal nitrates hydrates in the starting materials. On the curve, an obviously exothermic peak appears at a temperature of 330 °C, which is attributed to the decomposition of $1.5Gd(NO_3)_3{\cdot}3.5H_2O{\cdot}GbONO_3$ and $Yb(NO_3)_3{\cdot}H_2O{\cdot}YbONO_3$. Another exothermic peak at a temperature of 437 °C is ascribed to the decompositions of $GdONO_3$ and $YbONO_3$.[20,21] The strong exothermic peak at about 635 °C corresponds to the ending temperature of the large weight loss region. The large endothermic peak at 654 °C indicates that the new crystal phase begins to form at this temperature. In the third stage, the weight begins to keep invariable when the temperature exceeds 665 °C, which implies that the precursor decomposition and reaction have been completed and the crystal phase of Gd_6MoO_{12} has formed.

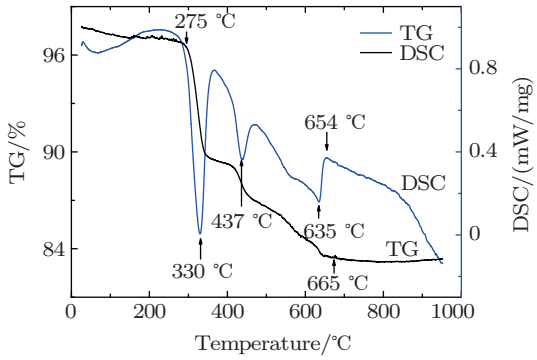


Fig. 3. (color online) TG-DSC curves of Gd_6MoO_{12}:Yb^{3+}/Tm^{3+} (sample A).

3.3. Luminescence properties of $Gd_{5.74}MoO_{12}$:0.25Yb^{3+}, 0.01Tm^{3+} phosphor

Figure 4 shows the UCL spectra and the morphologies of samples synthesized under different conditions. The dendrites display a prism, spindle, and sphere respectively, with sizes decreasing sequentially from sample A to sample C. Under the excitation of 980 nm, by comparing the UCL spectra of samples A, B, and C, we can see that with the particle size of the phosphors increasing, its UCL intensities increase dramatically. We know that the particle size of the phosphor

can affect the upconversion luminescence intensity.[22,23] This phenomenon may be attributed to the relatively large surface-to-volume ratio and few inner defects of microcrystals compared with those of bulk materials. In addition, the prisms have higher crystallinity and lower defect concentration than spheres and spindles, which also contribute to its stronger red and blue emission. Since "defects" are produced in the preparation process, which act as quenching centers (traps), when an excited luminescent center is in the vicinity of a trap, the excited energy can be transferred easily to the trap non-radiatively,[19] giving rise to the decreasing of luminescence intensity. When precursor A is annealed at a temperature of 700 °C for 4 h, sample A is obtained. Its crystal structure is broken as shown in Fig. 4(d). Meanwhile, the slight agglomerate phenomenon occurs, which is caused by the heating process, resulting in the further enhancement of the UC emission.

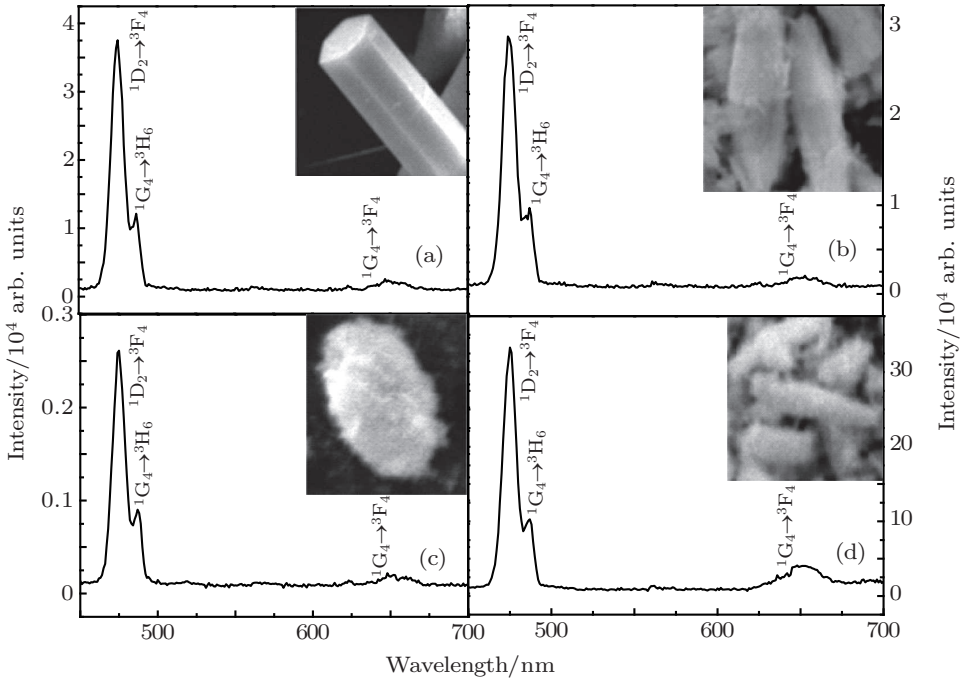


Fig. 4. UCL spectra pumped by a 980-nm diode laser for Gd_6MoO_{12}:0.25Yb^{3+}/0.01Tm^{3+} synthesized under different conditions: (a) pH = 3; (b) pH = 9; (c) pH = 3/EDTA; (d) annealed at the temperature of 700 ° for 4 hours of sample A.

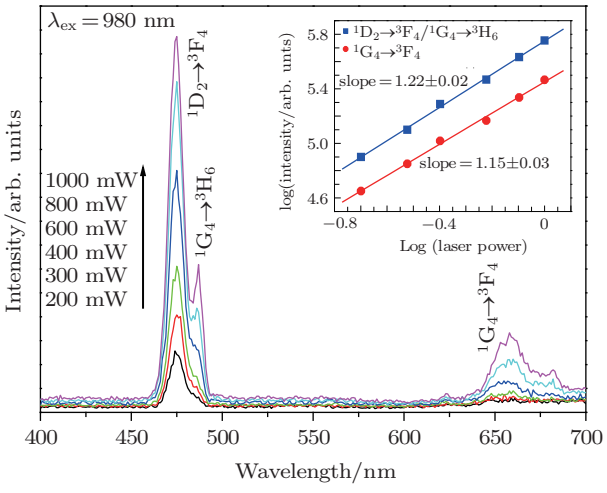


Fig. 5. (color online) Power dependences of UCL intensities of $^1G_4 \rightarrow {}^3H_6$, $^1D_2 \rightarrow {}^3F_4$, and $^1G_4 \rightarrow {}^3F_4$ emissions of sample A under 980-nm diode laser pump.

To understand the effect of pump power density on luminescence properties, the pump power-dependent UC curves are given in Fig. 5. The two-photon process corresponding to the red emission, has been discussed in many reports.[24] However, the calculated blue emission is a two-photon process, which is different from the typical three-photon process. This may be due to the competition between the linear decay and up conversion of the excited states, resulting in n becoming smaller than the theoretical value under high excited pump power.[25,26]

The mechanisms of Yb^{3+} as a sensitizer and Tm^{3+} as an activator UC luminescence system have been discussed widely in many researches.[27–29] The relative diagram can be seen in Fig. 6. The Yb^{3+} ion is a good sensitizer which can greatly enhance UC efficiency through energy transfer.[30] The three-photon process of blue emission produced by Tm^{3+} can be explained by the three successive energy transfers from Yb^{3+} to Tm^{3+} and the two-photon process of red emission can be explained by the two successive energy transfers from Yb^{3+} to Tm^{3+}. According to the Suyver *et al.* report,[26] the value of n deviating from the typical data is due to the competition between the linear decay and up conversion of the excited states. For blue emission, the value of n is 3, indicating the linear decay of the intermediate state is dominant. While n is 1 or 2, the

UC is dominant in the Yb^{3+}/Tm^{3+} co-doped system.[31] The red emission follows the same regularity.

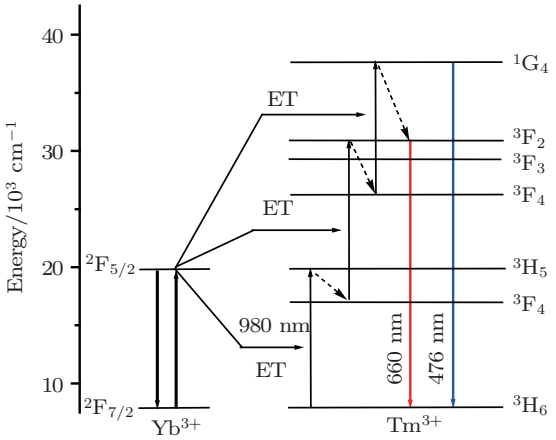


Fig. 6. (color online) Schematic energy levels of Yb^{3+} and Tm^{3+} ions in the as-prepared Gd_6MoO_{12}:Yb^{3+}/Tm^{3+} sample.

4. Conclusions

In this paper, Yb^{3+}/Tm^{3+} co-doped Gd_6MoO_{12} phosphors are synthesized successfully by the hydrothermal method. When changing the reaction conditions (pH, EDTA), various morphologies are observed, illustrating that the pH values and EDTA both play fundamental roles in the crystal growth. The luminescence properties of the samples are investigated in detail and its corresponding luminescence spectrum is measured and analyzed. Moreover, the results prove that the heating process has an effect on increasing the phosphor's crystallinity and producing an agglomerate phenomenon, further enhancing the UC emission. Finally, the mechanism of the UC luminescence is given. We believe that the work could provide some useful information for future research.

References

[1] Chen Z, Chen H, Hu H, *et al.* 2008 *J. Am. Chem. Soc.* **130** 3023
[2] Wang G, Peng Q and Li Y 2010 *Chem. Commun.* **46** 7528
[3] Zhou J, Liu Z and Li F 2012 *Chem. Soc. Rev.* **41** 1323
[4] Liang H, Lawrence N, Jones T, *et al.* 2007 *J. Am. Chem. Soc.* **129** 6068
[5] Li J, Hao Z, Zhang X, *et al.* 2012 *J. Colloid Interface Sci.* **392** 206
[6] Liu Y S, Tu D T, Zhu H M and Chen X Y 2013 *Chem. Soc. Rev.* **42** 6924
[7] Qin W P, Liu Z Y, Sin C N, *et al.* 2014 *Light: Science & Applications* **3** e193
[8] Sun J Y, Xian J B and Du H Y 2011 *J. Phys. Chem. Solid* **72** 207
[9] Xia Z G, Zhou W, Du H and Sun J 2010 *Mater. Res. Bull.* **45** 1199
[10] Wang J, Jing X, Yan C, Lin J and Liao F 2006 *J. Lumin.* **121** 57
[11] Lei F and Yan B 2008 *J. Solid State Chem.* **181** 855
[12] Shao W, Hua R, Zhang W, *et al.* 2013 *Powder Technol.* **23** 7326
[13] Pan C L, Liu H L, Guo Y, *et al.* 2014 *Acta Phys. Sin.* **63** 154211 (in Chinese)
[14] Li C, Quan Z, Yang J, Yang P and Lin J 2007 *Inorg. Chem.* **46** 6329
[15] Laudise R and Ballman A 1960 *J. Phys. Chem.* **64** 688
[16] Li W, Shi E and Fukuda T 2003 *Cryst. Res. Technol.* **38** 847
[17] Qiu H, Chen G, Sun L, *et al.* 2011 *J. Mater. Chem.* **21** 17202
[18] Yi G, Lu H, Zhao S, *et al.* 2004 *Nano Lett.* **4** 2191
[19] Sun Y, Chen Y, Tian L, *et al.* 2007 *Nanotechnology* **18** 275609
[20] Gao S L, He S Y, Jiang X W, *et al.* 1990 *Zhongguo Xitu Xuebao* **8** 277 (in Chinese)
[21] Du H Y, Sun J F, Xia Z G and Sun J Y 2009 *J. Electrochem. Soc.* **156** J361
[22] Chen Y S, Hao X L, Zhou J P, *et al.* 2012 *Mater. Lett.* **83** 49
[23] Jiang T, Qin W P and Zhao D 2012 *Mater. Lett.* **74** 54
[24] Gong L, Ma M, Xu C, Li X, Wang S, Lin J and Yang Q 2013 *J. Lumin.* **134** 718
[25] Pollnau M, Gamelin D, Lüthi S, *et al.* 2000 *Phys. Rev. B* **61** 3337
[26] Suyver J, Aebischer A, García-Revilla S, *et al.* 2005 *Phys. Rev. B* **71** 125123
[27] He E J, Liu N, Zhang M L, *et al.* 2012 *Chin. Phys. B* **21** 073201
[28] Xu Y L, Wang Y L, Shi L S and Tan X 2013 *Chin. Phys. Lett.* **30** 084207
[29] Huang S, Wang D, Wang Y, *et al.* 2012 *J. Alloys Compd.* **529** 140
[30] Luo Y, Xia Z G and Liao L B 2012 *Ceram. Int.* **38** 6907
[31] Wang G, Qin W, Wang L, *et al.* 2009 *J. Rare Earths* **27** 394